# 3 Results

This chapter summarises a number of results obtained over the past 12 years. Each section describes in detail one or two of the most pertinent results achieved and a few other accomplishments are also outlined.

## 3.1 Neutron stars

### 3.1.1 Constraining the neutron star equation of state using quiescent low mass X-ray binaries in globular clusters

Following the work done by Heinke et al. (2006) on Chandra data of the quiescent neutron star X-ray binary X7 in 47 Tucanae, we applied recently improved neutron star atmosphere models, available in a recent release of the *XSPEC* spectral fitting package (version 12.3.0, Arnaud, 1996), to three neutron stars in quiescent X-ray binaries that we have observed in three globular clusters with XMM-Newton. This was as a part of an on-going program to locate, identify and classify faint X-ray sources in globular clusters, undertaken in large part by myself and my PhD student Mathieu Servillat (Servillat et al., 2008b,a; Gendre et al., 2003b,a; Webb et al., 2004c, 2006), with an aim to determining the internal energy source that slows down the inevitable collapse of globular clusters, see Sec. 2.3.1. Early fitting of the X-ray spectra with the first hydrogen-atmosphere models of Zavlin et al. (1996) assuming a constant surface gravity (log $g_s$=14.385, corresponding to a 1.4 $M_\odot$ and 10 km radius neutron star), were reported for $\omega$ Cen and M 13 in Gendre et al. (2003b,a). However, as emphasised by Heinke et al. (2006), using models with appropriate surface gravity for each fitted value of the mass and radius of the neutron star is important when interpreting high quality X-ray spectra, which is indeed the case for the spectra measured with XMM-Newton. The three different hydrogen atmosphere models used were the basic neutron star atmosphere model (*nsa*) that we used previously in Gendre et al. (2003b,a). This model includes a uniform surface (effective) temperature, either a non-magnetised neutron star or with a field B = $10^{12}$ or B = $10^{13}$ G and a radiative atmosphere in hydrostatic equilibrium. The *nsagrav* model used is similar, but allows for a variety of surface gravitational accelerations, ranging from $10^{13}$ to $10^{15}$ cm $s^{-2}$, adapted to the masses and radii investigated. Finally we use the *nsatmos* model described by Heinke et al. (2006). This model includes a range of surface gravities and effective temperatures, and incorporates thermal electron conduction and self-irradiation by photons from the compact object. It also assumes negligible (less than $10^9$ G) magnetic fields and a pure hydrogen atmosphere.

For each neutron star, we fitted the spectrum obtained from all three *XMM-Newton* cameras simultaneously. However, for the neutron star in M 13 we also included the ROSAT PSPC archival observations of this source in M 13 (Verbunt, 2001) as in Gendre et al. (2003a), as the ROSAT data

Table 3.1: Results from spectral fitting for three neutron stars with three different hydrogen atmosphere model.

| Cluster | NSA | NSAGRAV | NSATMOS | $L_{bol}$ (erg $s^{-1}$) |
|---|---|---|---|---|
| $\omega$ Cen | $N_H$=$0.12\pm^{0.04}_{0.02}$ | $N_H$=$0.11\pm^{0.05}_{0.03}$ | $N_H$=$0.12\pm^{0.04}_{0.02}$ | $4.91 \times 10^{32}$ |
| | $log(T)$=$5.99\pm^{0.30}_{0.04}$ | $log(T)$=$5.99\pm^{0.20}_{0.11}$ | $log(T)$=$5.98\pm^{0.33}_{0.10}$ | |
| | $M$=$1.76\pm^{0.74p}_{1.26p}$ | $M$=$1.40\pm^{1.1p}_{1.10p}$ | $M$=$1.66\pm^{0.84}_{1.16p}$ | |
| | $R$=$11.30\pm^{7.27}_{6.30p}$ | $R$=$10.00\pm^{7.80}_{4.00p}$ | $R$=$11.66\pm^{7.03}_{4.99}$ | |
| | Cstat= 91.28, 85 dof | Cstat= 91.26, 85 dof | Cstat= 91.35, 85 dof | |
| M 13 | $N_H$=$0.013\pm^{0.005}_{0.005}$ | $N_H$=$0.013\pm^{0.005}_{0.004}$ | $N_H$=$0.012\pm^{0.004}_{0.003}$ | $5.08 \times 10^{32}$ |
| | $log(T)$=$6.00\pm^{0.01}_{0.01}$ | $log(T)$=$6.00\pm^{0.04}_{0.02}$ | $log(T)$=$6.00\pm^{0.01}_{0.09}$ | |
| | $M$=$1.38\pm^{0.08}_{0.23}$ | $M$=$1.39\pm^{0.51}_{0.67}$ | $M$=$1.30\pm^{0.06}_{0.12}$ | |
| | $R$=$9.95\pm^{0.24}_{0.27}$ | $R$=$9.95\pm^{2.21}_{0.36}$ | $R$=$9.77\pm^{0.09}_{0.29}$ | |
| | $\chi^2_\nu$=1.10, 62 dof | $\chi^2_\nu$=1.10, 62 dof | $\chi^2_\nu$=1.08, 62 dof | |
| NGC 2808 | $N_H$=$0.17\pm^{0.05}_{0.09}$ | $N_H$=$0.18\pm^{0.11}_{0.07}$ | $N_H$=$0.16\pm^{0.14}_{0.05}$ | $1.02 \times 10^{33}$ |
| | $log(T)$=$6.04\pm^{0.07}_{0.14}$ | $log(T)$=$6.08\pm^{0.06}_{0.17}$ | $log(T)$=$6.03\pm^{0.01}_{0.25}$ | |
| | $M$=$0.67\pm^{0.59}_{0.13}$ | $M$=$0.95\pm^{1.55p}_{0.65p}$ | $M$=$0.91\pm^{1.60}_{0.41p}$ | |
| | $R$=$8.45\pm^{0.36}_{3.45p}$ | $R$=$7.48\pm^{3.57}_{1.48p}$ | $R$=$6.10\pm^{11.47}_{1.10p}$ | |
| | Cstat=17.59, 19 dof | Cstat=18.12, 19 dof | Cstat=16.95, 19 dof | |

The column density, $N_H$ is $\times 10^{22}$ $cm^{-2}$, the temperature (T) is given as the logarithm of the temperature in Kelvin, the masses are in solar units and the radii in kilometres. All errors are given at the 90% confidence limit for the one interesting parameter. To calculate the errors, the mass and distance were held fixed and all other parameters were allowed to vary, except when calculating the error on the mass, when the radius was held fixed. A 'p' after the error value indicates that the hard limit of the model was reached. The estimated unabsorbed bolometric luminosity for each neutron star is also given.

extends below the XMM-Newton data, down to 0.1 keV (only 11.5 ks of data exists in the archives for $\omega$ Cen, which is insufficient to improve our spectra. No data exist for NGC 2808). The principal goal of our spectral fitting is to self-consistently constrain the allowed space in mass and radius using our three neutron stars, but also to test the reliability and accuracy of the three models examined. Table 3.1 gives the best fits for each neutron star fitted with each of the three models, along with the best fitting values for the column densities, surface temperatures of the neutron stars, masses and radii. Errors are also given at the 90% confidence limit for the one interesting parameter. To calculate the errors, the mass and distance were held fixed and all other parameters were allowed to vary, except when calculating the error on the mass, when the radius was held fixed instead of the mass. We also give the estimated bolometric luminosity of the neutron star. We found that we did not require any additional parameters, such as lines or edges to fit these data. However, this may be due to the quality of the data, where deeper observations may reveal spectral features that will be useful to constrain the gravitational redshift at the NS surface (Brown et al., 1998; Rutledge et al., 2002).

Even if the *nsa* model is more accurate in constraining $R_\infty$ than the *nsatmos* and *nsagrav*

models, when calculating a range of neutron star masses and radii, we find that the *nsatmos* and *nsagrav* models are better adapted. We conclude that the use of fixed gravity models for testing neutron stars with a variety of masses and radii (and therefore gravities) is not strictly appropriate as previously indicated by Gänsicke et al. (2002) and Heinke et al. (2006).

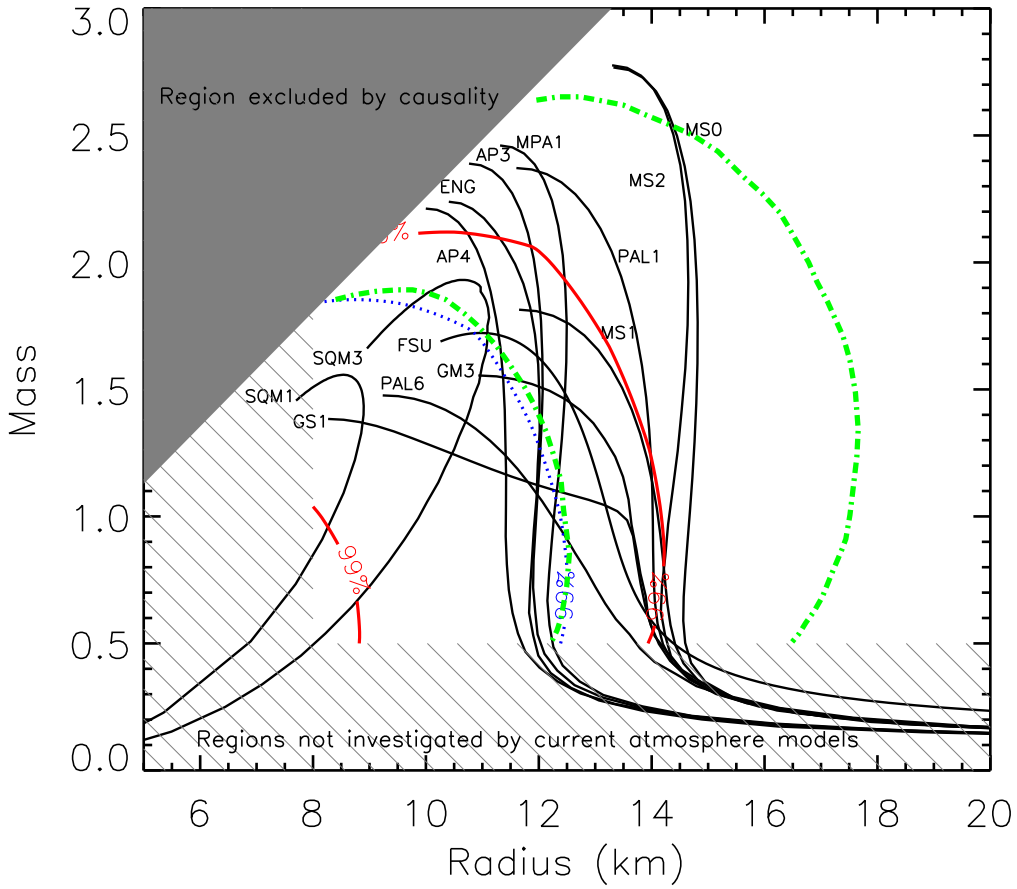


Figure 3.1: Contour plot showing the results of modelling the neutron stars in M 13 (dotted/blue line), $\omega$ Cen (solid/red line) and X7 in 47 Tuc (dashed-dotted/green line) (Heinke et al., 2006) with the xspec model *nsatmos*. The 99% confidence contours for the neutron star masses ($M_{\odot}$) and the radii (km) are plotted along with neutron star equations of state taken from Lattimer and Prakash (2007). The grey hashed region indicates the region not investigated with the models. The loci of models for the equations of state for dense matter are those described in Lattimer and Prakash (2007) and Lattimer and Prakash (2001) which include diverse equations such as: SQM - Prakash et al. (1995), a Strange Quark Matter model, PAL - Prakash et al. (1988) a neutron and proton model using a schematic potential, GM - Glendenning and Moszkowski (1991), a model containing neutrons, protons and hyperons using a field theoretical approach, GS - Glendenning and Schaffner-Bielich (1999), a model containing neutrons, protons and kaons using a field theoretical approach.

Using the results from fitting the neutron stars in M 13 and $\omega$ Cen, along with the results found by Heinke et al. (2006) when fitting Chandra observations of X7 in 47 Tuc, we show the allowed equations of state in Fig. 3.1. Modelling the neutron star in M 13 alone shows that the data do not

favour the stiffer equations of state, such as MS0-2 and PAL 1. We combine these results with those from modelling the neutron star in $\omega$ Cen. The low quality data for the neutron star in NGC 2808 results in very poor constraints for this object and hence we disregard this source in the discussion, although the results seem to be similar to those for the neutron star in M 13. The equations of state that are satisfied by all three neutron stars fall in the middle of the diagram and includes the equations of state of normal nucleonic matter and one strange quark matter model. The equations allowed are GS1, PAL 6, AP3 & 4, GM3, FSU, SQM3, ENG and MPA1, with masses up to 2.4 $M_{\odot}$.

### 3.1.2 High energy emission from pulsars

As described in Sec. 2.1.2, very few millisecond pulsars are detected in X-rays and fewer still show pulsations in this energy domain. Until recently, PSR J0218+4232 was the only MSP to show possible evidence for pulsations in $\gamma$-rays Kuiper et al. (2000). Much of my work has been consecrated to detecting millisecond pulsars in both the X-ray and $\gamma$-ray domain, with an aim to understanding the emission processes and constraining the neutron star equation of state, as outlined in Sec. 2.1.2.

Using *XMM-Newton* MOS imaging (0.2-10.0 keV) and pn timing (0.4-12.0 keV) data of PSR J0218+4232, we confirmed the previously detected pulsations of PSR J0218+4232 (Verbunt et al., 1996; Kuiper et al., 2002; Mineo et al., 2000) and we showed that the form of the lightcurve varies with energy (Webb et al., 2004a). We also showed that the broad band X-ray spectrum between 0.6-10.0 keV of the pulsed emission is softer than the spectrum measured between 2-10 keV using *BeppoSAX*, and provided some evidence that a simple power law may not be a good description of the 0.6-10.0 keV spectrum (Webb et al., 2004a). A similar analysis of the faint millisecond pulsars PSR J0751+1807 and PSR J1012+5307 revealed their X-ray spectra. We found that a power law model best fitted the spectrum of both MSPs. PSR J0751+1807 has a spectrum well fitted using a power law with photon index $\Gamma$=1.59$\pm$0.20, and an unabsorbed flux of 4.4 $\times 10^{-14}$ergs cm$^{-2}$s$^{-1}$ (0.2-10.0 keV). PSR J1012+5307 possibly has a similar spectrum $\Gamma$=1.78$\pm$0.36, with an unabsorbed flux of 1.2 $\times 10^{-13}$ergs cm$^{-2}$s$^{-1}$ (0.2-10.0 keV). However, a blackbody model cannot be excluded as the best fit to these data. We also showed evidence to suggest that both of these MSPs show X-ray pulsations, where PSR J0751+1807 appears to show a single pulse, and PSR J1012+5307 may show some evidence for two pulses per pulse period (Webb et al., 2004b).

We presented the first solid detection of a millisecond pulsar in the $\gamma$-ray domain (Abdo et al., 2009d), using the Large Area Telescope on the *Fermi Gamma-ray Space Telescope*. The discovery of PSR J0030+0451 revealed two narrow peaks, 0.07$\pm$0.01 and 0.08$\pm$0.02 wide, separated by 0.44$\pm$0.02 in phase. The derived chance occurrence probability of the null hypothesis, non-pulsed emission, was below $4\times10^{-8}$. The pulse shape is similar to that of the "normal" $\gamma$-ray pulsars. An exponentially cut-off power-law fit of the emission spectrum lead to an integral photon flux above 100 MeV of (6.76$\pm$1.05$\pm$1.35) $\times$ $10^{-8}$ cm$^{-2}$ s$^{-1}$ with cut-off energy (1.7$\pm$0.4$\pm$0.5) GeV (Abdo et al., 2009d). We then showed that this was in fact one of a number of $\gamma$-ray emitting MSPs, when we revealed a

total of 8 $\gamma$-ray MSPs detected with the *Fermi* LAT (Abdo et al., 2009a) J0030+0451, J0218+4232, J0437-4715, J0613-0200, J0751+1807, J1614-2230, J1744-1134 and J2124-3358, all with at least $5\sigma$ significance. Each pulsar shows evidence for two peaks and gamma-ray spectra best fitted with an exponentially cut-off power law ($\Gamma < 2$), with cut-off energies in the range 1-4 GeV. The spin-down powers ($\dot{E}$) of all the detected millisecond and normal gamma-ray pulsars lie above a common threshold of $\sim 5 \times 10^{33}$ ergs s$^{-1}$ kpc$^{-2}$. Most importantly, we showed that polar cap MSP models, where the bulk of the emission originates near the surface of the neutron star, predict that the pulsed gamma rays are roughly aligned with the magnetic poles. In outer gap (OG) and slot gap (SG) models, the bulk of the emission originates in the outer magnetosphere in narrow gaps along the last open field lines, forming wide fan beams that are not aligned with the magnetic poles. In the MSP $\gamma$-ray light curves detected, we found that although some of the $\gamma$-ray peaks are aligned with the radio peaks that are thought to be aligned with the magnetic poles, most are not. This points towards the outer-magnetosphere model geometry as a mechanism for producing the high energy emission from these pulsars. However, only MSPs with the highest spin-down power have a high enough electric potential for electron-positron pair production. Most of the MSPs detected by Fermi are below this threshold. Thus, some revision of the outer-magnetosphere models is needed. Surface magnetic fields may be stronger than assumed, perhaps because of magnetic multipoles or more compact neutron stars. Alternatively, the magnetic field at the light cylinder may play a greater role in particle acceleration than has been assumed.

From this work it appears important that the X-ray, $\gamma$-ray and radio lightcurves are examined contemporaneously. In conjunction with my PhD student Benoit Pancrazi, we therefore examined *XMM-Newton* data of PSR J0613-0200, PSR J1600-3053, PSR J1911-1114, PSR J2129-5721 and PSR J1853+1303, as well as complementary $\gamma$-ray and radio observations performed with the *Fermi* Large Area Telescope and the *Nançay* and *Parkes* radio telescopes (Pancrazi et al., 2011a). We showed significant pulsed $\gamma$-rays from PSR J1600−3053. The lightcurve determined for PSR J1600−3053 is similar to other MSPs. The exponential powerlaw spectral fit suggests a rather hard $\gamma$-ray source. However, the field is rather crowded and thus the fit may be sensitive to nearby sources and subject to systematic uncertainties related to the modelling of the overwhelming diffuse Galactic emission. The $\gamma$-ray spectrum of PSR J0613−0200 is consistent with outer magnetospheric emission (Cheng and Zhang, 1998; Zhang and Harding, 2000), also favoured by the detailed high-energy modelling performed by Venter et al. (2009) and as proposed by Abdo et al. (2009b). The sparse X-ray counts for PSR J0613−0200 do not allow us to distinguish between different spectral models. These five millisecond pulsars are amongst the thirty MSPs outside of globular clusters with the highest values of $B_{LC}$, the magnetic field strength at the light cylinder, as listed in the ATNF database (Manchester et al., 2005). We selected these five following arguments by Saito et al. (1997) that high $B_{LC}$ favours high-energy emission. Indeed, eleven of the thirty high $B_{LC}$ MSPs have been detected with *Fermi*. It should be noted, however, that seven of these $\gamma$-ray MSPs have distance values based on parallax measurements of less than $\sim$1 kpc, and that the remaining four have either very large $B_{LC}$ values

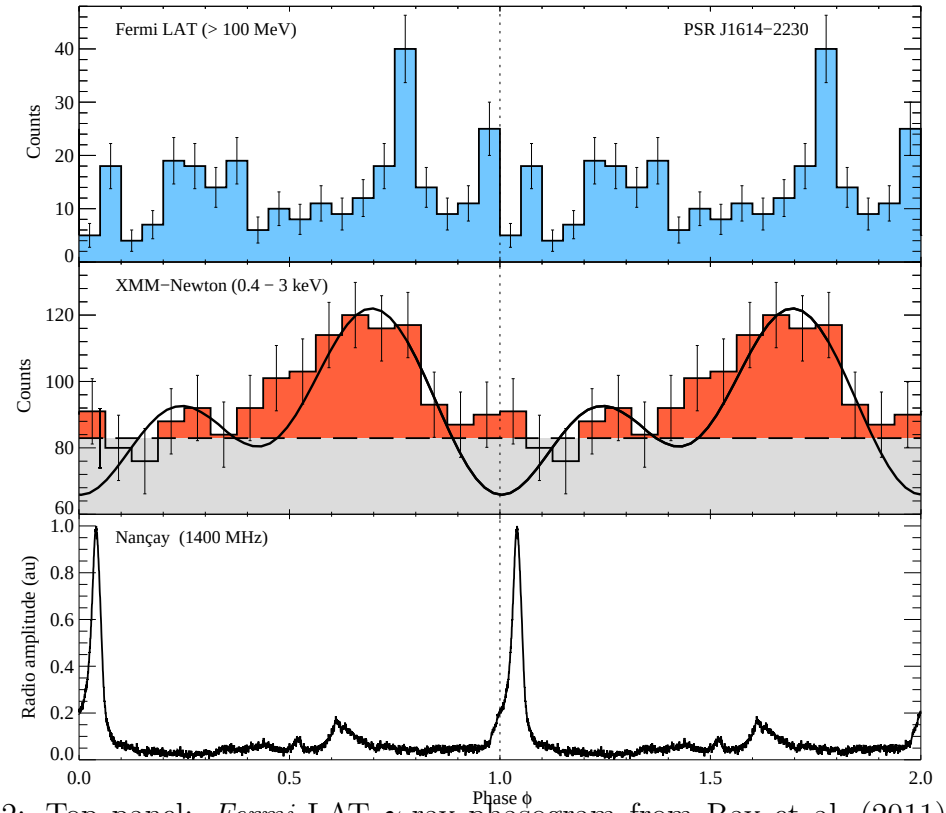


Figure 3.2: Top panel: *Fermi* LAT $\gamma$-ray phasogram from Ray et al. (2011), 20 bins per period. Middle: pn X-ray lightcurve of J1614−2230 (0.4−3.0 keV) overplotted with the model and parameters described in Sec. 3.1.2 (black solid line). The phasogram is shown with 16 bins per period and the dotted line corresponds to the background level. The error bars indicate the statistical 1 $\sigma$ error. Bottom: The Nançay 1400 MHz radio lightcurve. All plots show absolute phase.

($> 3{\times}10^5$ G) or distances based on the NE2001 model. Thus, the detections at high energies of PSR J0613−0200, the closest of the MSPs studied here and with a $B_{LC}$ slightly higher than the others, and of PSR J1600−3053 support the hypothesis of Saito et al. (1997). The non-detection of the other three, combined with the high significance detection of some closeby, bright MSPs with even lower values of $B_{LC}$, such as PSR J0437−4715 ($2.9{\times}10^4$ G) or PSR J0030+0451 ($1.8{\times}10^4$ G) show that the distance should also be taken into account when predicting the high-energy detectability. Alternatively, the $\gamma$-ray MSP results in Abdo et al. (2009b) suggest that $\dot{E}\ /d^2 > 5 \times 10^{33}$ erg s$^{-1}$ kpc$^{-2}$ is strongly correlated with high-energy detectability. Again, PSR J0613−0200 has the highest value ($\sim 5 \times 10^{34}$ erg s$^{-1}$ kpc$^{-2}$), yet PSR J1600−3053 has only $\dot{E}\ /d^2 \sim 3{\times}\ 10^{33}$ erg s$^{-1}$ kpc$^{-2}$ , with the other three MSPs having intermediate values. This suggests that these criteria must be used with some caution. Note also that $E\ /d^2$ is very sensitive to large uncertainties on the distance. Becker and Trümper (1997) showed results suggesting that the spin-down power is converted to X-rays with an efficiency of roughly $10^3$. Our value for PSR J0613−0200 as well as the four other upper limits all fall close to this line. In $\gamma$-rays, the conversion efficiency of spin-down power is high compared to X-rays (e.g. Abdo et al., 2009b; Zavlin, 2007), one reason why so many more MSPs have now been detected in $\gamma$-rays since the launch of the very sensitive *Fermi* LAT. This specificity combined with Fermi's survey capability accumulating data over the whole sky makes the $\gamma$-ray domain essential

for improving our understanding of the high-energy emission coming from MSPs.

More recently we have also analysed two newly detected $\gamma$-ray pulsars, PSR J1459−6053 and PSR J1614−2230, in the X-ray domain with *XMM-Newton* to try to enlarge the sample of pulsars for which multi-wavelength data exists (Pancrazi et al., 2011b). J1459−6053 shows X-ray spectra best fitted with a power law model, with a photon index, $\Gamma$=$2.10^{+1.24}_{-0.85}$ , suggesting non-thermal magnetospheric emission like that observed from the $\gamma$-ray data. Analysis of the X-ray lightcurve folded on the $\gamma$-ray ephemeris shows modulation at the 3.7 $\sigma$ level in the 1.0−4.5 keV domain. Possible alignment of the main $\gamma$-ray and X-ray peaks further supports the interpretation that the emission in the two energy domains emanates from similar regions. The millisecond pulsar J1614−2230 exhibits an X-ray spectrum with a substantial thermal component, where the best fitting spectral model is either two blackbodies, with kT=$0.14^{+0.05}_{-0.02}$ and $0.80^{+1.90}_{-0.32}$ keV or a blackbody with similar temperature to the previous cooler component, kT=$0.13^{+0.04}_{-0.02}$ keV and a power law component, with a photon index, $\Gamma$=$1.15^{+1.84}_{-1.65}$. The cooler blackbody component is likely to originate from the hot surface at the polar cap. Analysis of the X-ray lightcurve folded on the radio ephemeris shows modulation at the 4.0 $\sigma$ level in the 0.4−3.0 keV domain. If the best fit is determined to be thermal in nature, through analysis of better quality data, then the X-ray data can be modelled in a similar way to Bogdanov et al. (2007) and $\gamma$-ray and radio data can also be exploited to constrain the neutron star equation of state. Venter et al. (2009) modelled the $\gamma$-ray and radio data and found that the $\gamma$-ray emission is likely to come from the outer gap and proposed a magnetic inclination ($\alpha$) of $\sim$40° and a viewing angle relative to the rotation axis ($\zeta$) of $\sim$80°. These are approximate values and no formal errors are associated with these estimates. None the less, we can take these estimates at face value and use them in a model like that presented by Bogdanov et al. (2007). The model considers thermal X-ray emission emanating from the polar caps of a neutron star through a non-magnetised light element atmosphere (*nsagrav* in *Xspec*, Zavlin et al., 1996). This model includes all the relativistic corrections necessary for such a compact star. We also include the mass derived by Demorest et al. (2010), see Section 2.1.2. This leaves only the radius of the neutron star and the configuration of the dipolar magnetic field as free parameters. Due to the low signal to noise of the X-ray lightcurve, detailed modelling is excluded and so we use the model in an illustrative manner only. We can see that the observed lightcurve can indeed be described by including the estimates proposed by Venter et al. (2009) and a neutron star with the high mass of Demorest et al. (2010), in Fig. 3.2. The general form of the X-ray lightcurve can be described using these parameters and an offset dipole, again similar to that used by Bogdanov et al. (2007) to model PSR J0437−4715 and a radius $\gtrsim$12 km. The inclusion of the offset dipole is interesting as it is one of the methods that Venter et al. (2009) use to explain the $\gamma$-ray emission observed from MSPs, where the low MSP magnetic field inhibits the creation of sufficient electron-positron pairs which are ultimately responsible for the $\gamma$-ray emission.

## 3.2 Globular clusters

To address some of the problematics presented in Section 2.3 regarding globular clusters, I have observed nine Galactic globular clusters with *XMM-Newton*, in collaboration with my PhD student Mathieu Servillat and Masters students Denis Serre and Daniel Seguignes, $\omega$ Cen (Gendre et al., 2003b), M 13 (Gendre et al., 2003a), NGC 6636 (Webb and Barret, 2005), M 22 (Webb et al., 2004c, 2002), M 55 (Webb et al., 2006), NGC 3201(Webb et al., 2006), NGC 2808 (Servillat et al., 2008b,a), NGC 4372 (Servillat et al., 2008b) and M 69. We also have optical photometry, optical spectroscopy, radio imaging and Chandra data for a number of these clusters. Thanks to the multi-wavelength data we have been able to detect and identify many new binary systems and their products, which are expected to exist due to the age of the clusters coupled with their high dynamical encounter rate, see Section 2.3. I outline a few of the most interesting results from our studies here.

Kundu et al. (2003) found that metal-rich extragalactic GCs host three times as many low mass X-ray binaries than metal-poor ones. From in depth studies of the number of CVs in NGC 2808, compared to observations of similar globular clusters (47 Tuc and M 80) and models (Pooley and Hut, 2006; Ivanova et al., 2006) we deduced that NGC 2808 is deficient in CVs and this is likely to be due to the low metallicity of this cluster (Servillat et al., 2008a).

Using X-ray (*XMM-Newton* and *Chandra*) and optical photometry (*Faulkes Telescope* monitoring and *Hubble Space Telescope*) we identified and examined a new CV (dwarf nova) in M 13 (Servillat et al., 2011b). Using the same X-ray observatories and *VLT* FORS2 spectroscopy, we examined another in M 22 (Webb and Servillat, 2011). Recently, it has been proposed that it may not simply be the magnetic field that is responsible for the lack of outbursts. Dobrotka et al. (2006) suggest that it may be due to a combination of low mass transfer rates ($\lesssim 10^{14-15}$ g s$^{-1}$) and moderately strong white dwarf magnetic moments ($\gtrsim 10^{30}$ G cm$^3$) which could stabilise the CV discs through truncation of inner regions (Meyer and Meyer-Hofmeister, 1994) and thus prevent most of them from experiencing frequent outbursts. Ivanova et al. (2006) has also suggested that the lack of outbursts are due to higher white dwarf masses in GC CVs compared to those in the field. This would imply that GC CVs are intrinsically different to those in the field. This could be due to the difference in the formation mechanisms of GC and field CVs, where a substantial fraction of cluster CVs are likely to be formed through encounters, rather than from their primordial binaries (Ivanova et al., 2006). Alternatively, the observed phenomenon could simply be due to selection biases, where our knowledge of CVs is limited to a small population of the closest CVs that are frequently observed to outburst, as these are the easiest objects to detect. Further, it has recently been proposed that the majority of CVs may be short period, low mass transferring systems that therefore show infrequent outbursts (e.g. Uemura et al., 2010). If this is the case, GC CVs may be no different to the field CV population. The CVs studied in M 13 and M 22 both seem to suggest short period, low mass transferring systems with infrequent outbursts. This could then go some way to supporting the idea that the dearth of outbursts in globular clusters is indeed because the majority of CVs have such

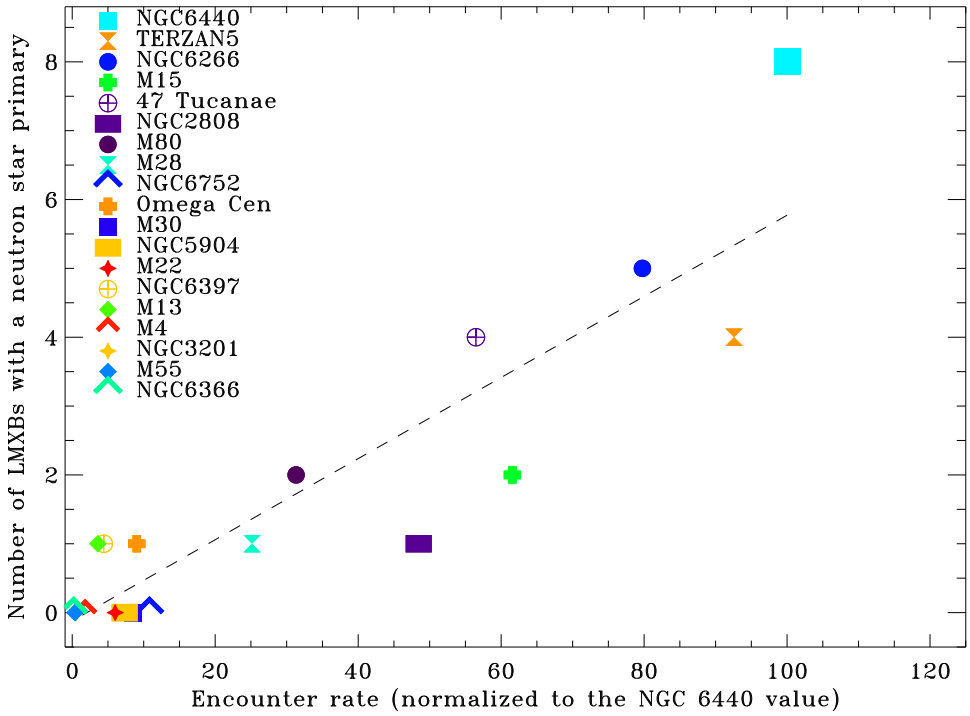


Figure 3.3: The number of quiescent neutron stars versus encounter rate ($\rho_0^{1.5} r_c^2$), shown with a linear fit, adapted from Gendre et al. (2003a). The encounter rates have been normalized to 100 for NGC 6440.

characteristics (Uemura et al., 2010). This observed dearth is then related to selection biases.

As the faintest detection limit of all the *XMM-Newton* and *Chandra* observations of globular clusters ($\sim 10^{29}$-$10^{31}$ erg s$^{-1}$) is considerably fainter than the minimum luminosities of qNSLMXBs ($\sim 10^{32}$ erg s$^{-1}$), we can consider that the populations of qNSLMXBs detected in each globular cluster are (almost) complete (although source confusion could mar the completeness Heinke et al., 2003, or some qNSLMXBs may show hard X-ray spectra and not be accounted for in this analysis).

Plotting the number of qNSLMXBs found with soft spectra against the globular cluster encounter rate, Gendre et al. (2003a) found that a correlation existed for the 10 globular clusters (containing 10-11 qNSLMXBs) that had been observed by either *XMM-Newton* or *Chandra* by 2003. The data could be fitted with a linear relation, although the numbers involved were low and therefore the statistical significance also low, see Fig. 3.3 for an updated version of the plot presented in Gendre et al. (2003a). These observations do support the idea that qNSLMXBs are formed through encounters, in a similar way to the NSLMXBs. Pooley et al. (2003) subsequently analysed 14 globular clusters, containing a total of 19-22 qNSLMXBs and found that this analysis also supported the idea that qNSLMXBs are formed in large part through encounters. They found that a power law fit with an index of 0.97±0.5 fitted the number of LMXBs versus the encounter rate, consistent with a linear relationship. Heinke et al. (2003) also support this hypothesis, using the density weighting method of Johnston and Verbunt (1996) and using an estimate for the incompleteness of qNSLMXBs detected in certain clusters.

As globular clusters are known to harbour a significant population of neutron star X-ray binaries that could be responsible for delaying the inevitable core collapse of these dense clusters, and taking into account the fact that they are old systems, their progeny, namely millisecond pulsars, should also be present in large numbers, see Section 2.3. Following the confirmation using the *Fermi* Gamma-ray Space Telescope that millisecond pulsars are indeed gamma-ray emitters (Section 3.1), we showed for the first time that the Galactic globular cluster 47 Tuc emits in the $\gamma$-ray domain and that the $\gamma$-ray spectrum is consistent with $\gamma$-ray emission from a population of millisecond pulsars. The observed $\gamma$-ray luminosity implies an upper limit of 60 millisecond pulsars present in 47 Tucanae. Until this work the study of close binary systems in globular clusters had mainly relied on X-ray observations. Such studies, however, are hampered by the fact that a large variety of binary systems emit X-rays and that it is difficult to assess the nature of the sources from X-ray observations alone. X-ray studies must therefore be backed up by multiwavelength identification programs that help to disentangle these source populations. High-energy $\gamma$-ray observations are unique in that they should be sensitive mainly to the pulsar populations. This is illustrated by *Fermi* observations of our own Galaxy that have revealed that pulsars form the largest and most luminous point-source population in this energy domain (Abdo et al., 2009c; Webb and Knödlseder, 2010).

We then analysed a further 13 Galactic globular clusters with *Fermi*. Steady point-like high-energy gamma-ray emission was significantly detected towards 8 globular clusters. Five of them (47 Tucanae, $\omega$ Cen, NGC 6388, Terzan 5, and M 28) showed hard spectral power indices ($0.7 < \Gamma < 1.4$) and clear evidence for an exponential cut-off in the range 1.0-2.6 GeV, which is the characteristic signature of magnetospheric emission from MSPs. Three of them (M 62, NGC 6440 and NGC 6652) also showed hard spectral indices ($1.0 < \Gamma < 1.7$), however the presence of an exponential cut-off could not be unambiguously established. Three of them ($\omega$ Cen, NGC 6388, NGC 6652) have no known radio or X-ray MSPs yet still exhibit MSP spectral properties. From the observed $\gamma$-ray luminosities, we estimated the total number of MSPs that is expected to be present in these globular clusters. We show that the number of MSP scales with encounter rate, in the same way as the neutron star X-ray binaries, reinforcing the link between these two objects. The number of MSPs scales as $0.5\Gamma + 18$, see Fig. 3.4. Using this relation, we estimated 2600-4700 MSPs in Galactic globular clusters, commensurate with previous estimates. This shows that the observation of high-energy $\gamma$-ray emission from globular clusters provides a reliable independent method to assess their millisecond pulsar populations and that such populations could be sufficient in slowing the core collapse of globular clusters (Abdo et al., 2010b, corresponding author).

## 3.3 Compact objects in the XMM-Newton catalogue, 2XMM

The *XMM-Newton* catalogue (Watson et al., 2009), *2XMM* (latest release, April 2010: 2XMMi-DR3) contains 262902 unique X-ray sources detected in 504 square degrees of sky and is the largest X-ray

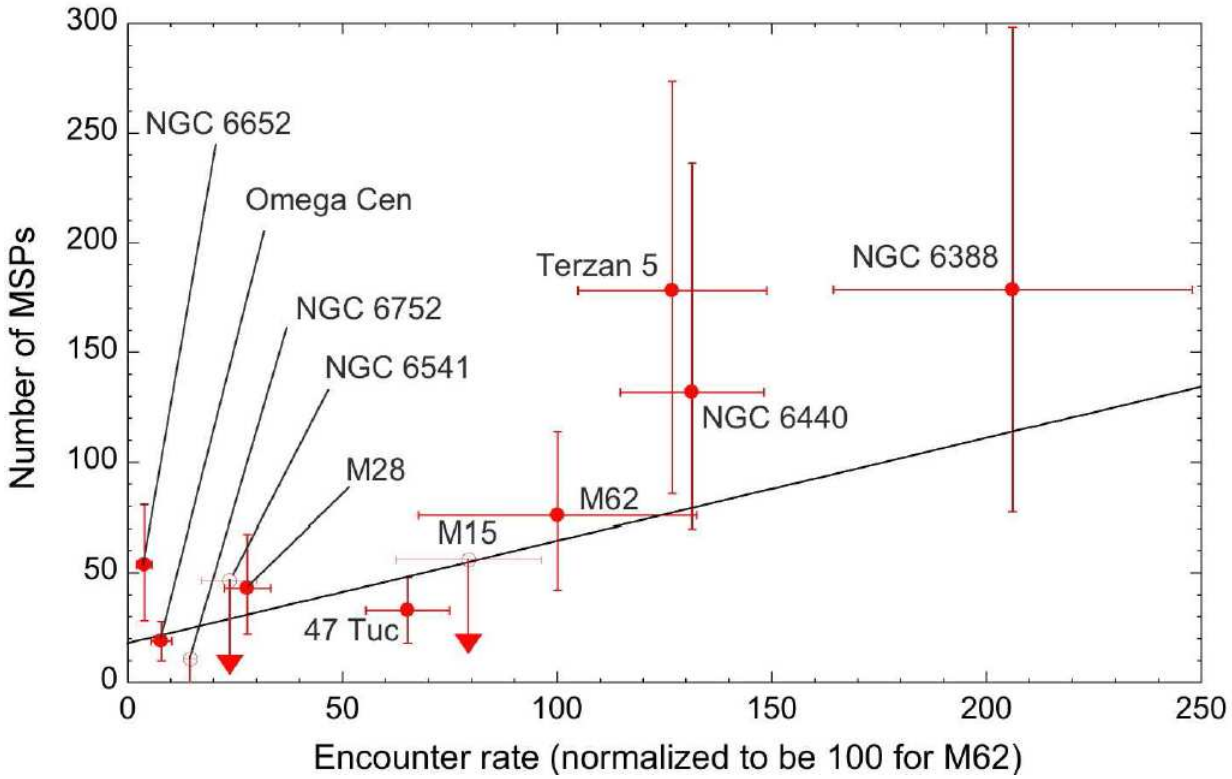


Figure 3.4: The predicted number of millisecond pulsars versus encounter rate ($\rho_0^{1.5} r_c^2$), shown with a linear fit, adapted from Gendre et al. (2003a). The encounter rates have been normalized to 100 for M 62.

catalogue to date. The median X-ray flux (in the energy band 0.2 - 12 keV) of the catalogue sources is $\sim 2.5 \times 10^{-14}$ erg cm$^{-2}$ s$^{-1}$, where $\sim$20% of the sources have fluxes below $1 \times 10^{-14}$ erg cm$^{-2}$ s$^{-1}$. The increased depth of the observations, compared to those made previously with *Rosat*, which had a limit of $\sim 2 \times 10^{-13}$ erg cm$^{-2}$ s$^{-1}$ assuming a power law with $\alpha$=3 (Rutledge et al., 2003), means many new faint X-ray sources are detected in *2XMM*. These X-ray sources are however, some of the most extreme objects in the Universe. Many of them are related to compact objects, namely white dwarfs, neutron stars and black holes which manifest themselves as cataclysmic variables, super soft sources, pulsars, magnetars, stellar mass black hole binaries, active galactic nuclei (AGN) or even intermediate mass black holes, for example. I have a programme conducted in collaboration with some SSC members and also with my post-docs (Sean Farrell and Dacheng Lin) and a number of Masters students (David Villa-Pascual, Joana Rodrigues, Damien Sossai and Stéphanie Dupuy) to systematically search the catalogue *2XMM* for interesting and extreme objects as described above. So far we have discovered a number of very interesting compact objects, which are described in this section.

Examining the 2XMM catalogue for sources outside the Galactic plane and undertaking optical spectroscopy of these sources revealed that the large majority are indeed galaxies containing super-massive black holes that are actively accreting material (AGN) (e.g. Barcons et al., 2002; Caccianiga et al., 2004; Barcons et al., 2007). Further, examining some apparently non-active galaxies (from optical observations) in the X-rays revealed an active nucleus. These results show that optical spec-

troscopy can sometimes be inefficient in revealing the presence of an AGN, which instead is evident using an X-ray spectroscopic investigation (Severgnini et al., 2003). These studies are essential for detecting the optically obscured population of AGN (Caccianiga et al., 2004; Barcons et al., 2007).

Focussing on objects in our own Galaxy reveals different source populations (Motch et al., 2010). Our optical campaign of the brightest X-ray sources in the *XMM-Newton* Galactic plane survey revealed that active coronae account for 16 of the 30 positively or tentatively identified X-ray sources and exhibit the softest X-ray spectra. Many of the identified hard X-ray sources are associated with massive stars, possible members of binary systems and emitting at intermediate X-ray luminosities of $10^{32-34}$ erg s$^{-1}$. Among these are (i) a very absorbed, likely hyper-luminous star with X-ray/optical spectra and luminosities comparable to those of $\eta$ Carina; (ii) a new X-ray-selected WN8 Wolf-Rayet star in which most of the X-ray emission probably arises from wind collision in a binary; (iii) a new Be/X-ray star belonging to the growing class of $\gamma$-Cas analogues; and (iv) a possible supergiant X-ray binary of the kind discovered recently by INTEGRAL. One of the sources, XGPS-25, has a counterpart of moderate optical luminosity that exhibits HeII $\lambda$4686Å and Bowen CIII-NIII emission lines, suggesting that this may be a quiescent or X-ray shielded low mass X-ray binary, although its X-ray properties might also be consistent with a rare kind of cataclysmic variable (CV). We also discovered three new CVs, one of which is a likely magnetic system displaying strong X-ray variability. The soft (0.4-2.0 keV) band log N(>S) - log S curve is completely dominated by active stars in the flux range of $1\times10^{-13}$ to $1\times10^{-14}$ erg cm$^{-2}$ s$^{-1}$. Several active coronae are also detected above 2 keV suggesting that the population of RS CVn binaries contributes significantly to the hard X-ray source population. In total, we were able to identify a large fraction of the hard (2-10 keV) X-ray sources with Galactic objects at a rate consistent with that expected for the Galactic contribution alone (Motch et al., 2010).

As result of some work with my post-doc Sean Farrell, we have also identified a new 626±2 s periodic X-ray source in the direction of the Galactic centre (Farrell et al., 2010). Spectral fitting showed that the spectrum is consistent with an absorbed power law. No significant spectral variability was observed over the 626 s period. We investigated the possibility that the 626 s period is orbital in nature (either that of an ultra-compact X-ray binary or an AM CVn) or related to the spin of a compact object (either an accretion powered pulsar or an intermediate polar). The X-ray properties of the source and the photometry of the candidate near-infrared counterparts are consistent with an accreting neutron star X-ray binary on the near-side of the Galactic bulge, where the 626 s period is most likely indicative of the pulsar spin period. However, we cannot rule out an ultra-compact X-ray binary or an intermediate polar with the data at hand. In the former case, if the 626 s modulation is the orbital period of an X-ray binary, it would be the shortest period system known. Based on the slow period and the photometry of the near-infrared counterparts, we instead suggest that 2XMM J174016.0-290337 could be a new addition to the emerging class of symbiotic X-ray binaries (Farrell et al., 2010).

Finally two specific sources discovered outside our Galaxy, thanks to work with my post-docs

(Sean Farrell and Dacheng Lin) and several masters students (David Villa-Pascual, Joana Rodrigues, Damien Sossai and Stéphanie Dupuy). The first is an ultrasoft X-ray transient source, 2XMMi J184725.1-631724, detected serendipitously in two *XMM-Newton* observations in the direction of the center of the galaxy IC 4765-f01-1504 at a redshift of 0.0353 (Lin et al., 2011). These two observations were separated by 211 days, with the 0.2-10 keV absorbed flux increasing by a factor of about nine. The spectra were best described by a model dominated by a thermal disk or a single-temperature blackbody component (contributing $\gtrsim$80% of the flux) plus a weak powerlaw component. The thermal emission has a temperature of a few tens of eV, and the weak powerlaw a photon index of $\sim$3.5. Similar to the black hole X-ray binaries in the thermal state, our source exhibited an accretion disk whose luminosity appears to follow the $L_v \propto T^4$ relation. This would indicate that the black hole mass is about $10^5$-$10^6$ $M_\odot$ using the best-fitting inner disk radius. Both *XMM-Newton* observations show variability of about 21% on timescales of hours, which can be explained as due to fast variations in the mass accretion rate. The source was not detected by *ROSAT* in an observation in 1992, indicating a variability factor of $\gtrsim$64 over longer timescales. The source was not detected again in X-rays in a *Swift* observation in February 2011, implying a flux decrease by a factor of $\gtrsim$12 since the last *XMM-Newton* observation. The transient nature, in addition to the extreme softness of the X-ray spectra and the inactivity of the galaxy implied by the lack of strong optical emission lines, makes it a candidate tidal disruption event. If this is the case, the first *XMM-Newton* observation would have been in the rising phase and the second one in the decay phase.

The final object, and currently the most intriguing object is 2XMM J011028.1-460421, referred to hereafter as HLX-1, was discovered serendipitously using *XMM-Newton* on 23 November 2004, in the outskirts of the edge-on spiral galaxy ESO 243-49, 8" from the nucleus yet within the confines of the galaxy (Farrell et al., 2009). At the distance of the galaxy ($z = 0.0224$; Afonso et al., 2005) the 0.2 – 10 keV unabsorbed X-ray luminosity, assuming isotropic emission, was found to be $1.1 \times 10^{42}$ ergs $s^{-1}$. A second XMM-Newton observation performed 4 years later on 28 November 2008 revealed that the source spectrum and X-ray luminosity had varied, ruling out multiple lower-luminosity sources as the origin of the X-ray emission. The observed steep X-ray spectrum and lack of radio counterpart made a background object unlikely. The X-ray spectrum and the faint optical counterpart ($R\sim$ 24.6 Soria et al., 2010), precluded objects such as a coronally active star, a supernova remnant, an accreting white dwarf or neutron star. The derived luminosity for HLX-1 at 10 kpc is only $10^{34}$ erg $s^{-1}$, too low for a Galactic black-hole binary undergoing near-Eddington accretion. In addition, the Eddington ratio implied by the observed luminosity (assuming a stellar mass BH) should easily accelerate matter to high Lorentz factors (Abramowicz et al., 1990), producing relativistic jets and a flat X-ray spectrum (Freeland et al., 2006). The observed steep spectrum thus also ruled out beaming as the origin of the high luminosity, leaving an IMBH as the most likely cause.

Using *VLT* FORS2 low resolution spectroscopy of the optical counterpart detected by Soria et al. (2010) we successfully deconvolved $H_\alpha$ emission emanating from HLX-1 from background $H_\alpha$ absorption arising from the host galaxy (Wiersema et al., 2010). The $H_\alpha$ emission redshift

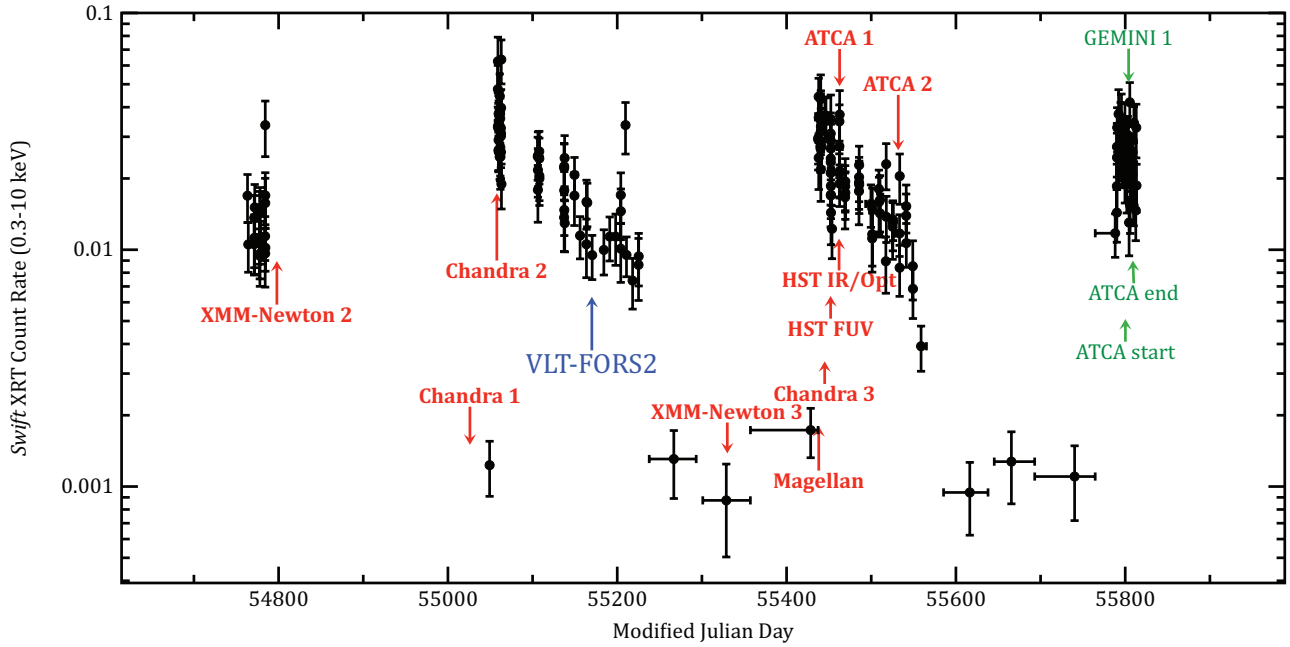


Figure 3.5: The Swift X-ray lightcurve of ESO 243-49 HLX-1, including some of our other complimentary multi-wavelength data.

is consistent with that of ESO 243-49. This finding definitively places HLX-1 inside ESO 243-49, confirming the extreme maximum luminosity and strengthening the case for it containing an accreting intermediate-mass black hole of more than $500M_{\odot}$, see Sec. 2.1.1.

Our regular monitoring of HLX-1 with *Swift*, see Fig. 3.5, has revealed significant flux changes in conjunction with simultaneous spectral changes in the same way as Galactic BH X-ray binaries (Godet et al., 2009; Servillat et al., 2011a), strengthening the case for an accreting BH in HLX-1. This is the first time that state transitions between the low/hard and the high/soft states have been seen in a ULX. HLX-1's spectral variability also argues against beaming as the origin of the extreme luminosity as only a hard spectrum would be expected (Freeland et al., 2006). It has become evident that HLX-1's X-ray variability follows a fairly distinct pattern over approximately 1 year (Lasota et al., 2011; Kong, 2011). Taking all of the observations to date, from 2004 with *XMM-Newton*, along with two *Rosat* observations at the beginning of the 90's, also supports such a regularity between outbursts.

Galactic black hole binaries are known to regularly emit radio flares around the transition from the low/hard to the high/soft state, e.g. Fender et al. (2009). These are associated with ejection events, where, for example, the jet is expelled which can lead to radio flaring when the higher velocity ejecta may collide with the lower-velocity material produced by the steady jet. We observed HLX-1 with the Australia Telescope Compact Array (ATCA) in the 750 m configuration on the 13th September 2010, when our regular X-ray monitoring of HLX-1 with the Swift satellite (Gehrels et al., 2004) showed that HLX-1 had just undergone a transition from the low/hard X-ray state to the high/soft X-ray state. As well as detecting radio emission from the nucleus of the galaxy, we detected

a radio point source at Right Ascension (RA) = $01^h10^m28.28^s$ and declination (dec.) = -46°04'22.3", coincident with the Chandra X-ray position of HLX-1 (Webb et al., 2010). Combining the 5 GHz and 9 GHz data gives a detection of 40 $\mu$Jy/beam, and a 1 $\sigma$ noise level of 9.5 $\mu$Jy, thus a 4.2 $\sigma$ detection at the position of HLX-1, at a time when such emission can be expected. To determine whether the radio emission that we detected was transient and thus associated with a radio flare, we made another observation with the ATCA in the 6 km configuration on 3rd December 2010, when HLX-1 was declining from the soft state and when no flaring is expected. This observation again showed emission from the nucleus of the galaxy, consistent with that of the previous radio observation, but revealed no source at the position of HLX-1. The 3 $\sigma$ non-detection for the combined 5 GHz and 9 GHz data is 33 $\mu$Jy/beam. The radio emission is therefore associated with a jet ejection event. This reinforces the idea that HLX-1 does indeed behave in a similar way to Galactic black holes binaries and these observations also support the scale invariance of jets, relating the mass accretion to the power output for black holes in all mass ranges, see Section 2.1.1.

The mass of the black hole in HLX-1 has been estimated through modelling of the X-ray spectra (Davis et al., 2011; Servillat et al., 2011a; Godet et al., 2011). These estimates cluster around $\sim 1\times10^4$ $M_\odot$, further supporting the intermediate mass black hole hypothesis. However, it is difficult to understand the variability that is observed from this object. We have tried to understand the X-ray/radio variability by drawing analogies with Galactic BH binaries. The X-ray data seem to indicate a FRED (Fast Rise Exponential Decay) lightcurve. This coupled with the spectral state variations suggest that the variability should result from the same thermal-viscous instability that drives the outbursts of Galactic BH binaries and dwarf-nova stars, and that the HLX-1 behaviour might be described by a variant of the corresponding disk instability model (DIM; see Sec. 2.2 and Lasota, 2001, for a review). We modelled the X-ray variations in the framework of the DIM, considering various scenarios such as an irradiation dominated disc or a radiation pressure dominated disc. However, the required size of the accretion disc is much too large to be compatible with the X-ray variability timescales observed, although we can not exclude that the variability is due to the instability that can arise in radiation-pressure dominated discs. We have shown, however, that a viable description of the variability can be provided by a model in which enhanced mass transfer into a quasi-permanent accretion disk is triggered by the passage at periastron of an evolved (AGB) star circling the IMBH in an eccentric orbit (Lasota et al., 2011). The recurrence time of $\sim$1 year is consistent with this hypothesis.

In addition, we have obtained FUV, NUV, C, V, I and H-band *Hubble* photometry along with *Swift* X-ray data at a similar time during the 2010 outburst. Modelling the data together indicates the presence of an (irradiated) accretion disc and a stellar population (Farrell et al. sub.), although there are large uncertainties due to the small number of data points compared to the complexity of the model. A young stellar population could be explained in an accreted dwarf galaxy scenario, whereby star formation is triggered via tidal interactions between the dwarf galaxy and ESO 243-49 (Knierman, 2010). Tidal stripping a dwarf galaxy during a merger could remove mass from this

system, leaving behind an IMBH embedded in the remnant of the nuclear bulge. This may go some way to understanding the origin of this rare and intriguing object, but much more work is required to gain a full picture.